Energy & Environmental Science

COMMUNICATION

View Article Online
View Journal | View Issue

Cite this: *Energy Environ. Sci.*, 2015, **8**, 3539

Received 7th August 2015,
Accepted 13th October 2015

DOI: 10.1039/c5ee02443a

www.rsc.org/ees

A new approach to prepare highly active and stable black titania for visible light-assisted hydrogen production†

Apurba Sinhamahapatra, Jong-Pil Jeon and Jong-Sung Yu*

In spite of their remarkable enhancement in visible light absorption, black TiO_2 materials have failed to demonstrate expected photocatalytic activity in visible light due to the presence of a high number of recombination centers. In this report, a new controlled magnesiothermic reduction has been developed to synthesize reduced black TiO_2 under a 5% H_2/Ar atmosphere. The material possesses an optimum band gap and band position, oxygen vacancies, surface defects, and charge recombination centers and shows significantly improved optical absorption in the visible and infrared region. The synergistic effects enable the black TiO_2 material to show an excellent hydrogen production ability in the methanol–water system in the presence of Pt as a co-catalyst. The maximum hydrogen production rates are 43 mmol h^{-1} g^{-1} and 440 μmol h^{-1} g^{-1}, along with remarkable stability under the full solar wavelength range of light and visible light, respectively, and these values are superior to those of previously reported black TiO_2 materials.

Broader context

One of the most important research areas in modern decades is the production of hydrogen from water using visible light owing to the energy crisis for the present and future generations. Photocatalytic water splitting is one of the easiest ways, but has been suffering from the lack of potential catalyst systems. Black TiO_2 is one of the promising catalysts for hydrogen production with astonishing light absorption in the full solar wavelength range of light compared to white TiO_2 (absorbs only UV light). Although its activity is remarkably improved under the full solar wavelength range of light and UV light, black TiO_2 fails to impress the world with its activity for visible light-assisted hydrogen production due to the presence of large amounts of recombination centers that are produced during synthesis. Different methods were used to prepare black TiO_2 to improve its visible light activity, but were limited to only a slight improvement. In this work, a new approach has been developed to achieve highly efficient and remarkably stable black TiO_2 that outperforms the previous reported black TiO_2 in terms of hydrogen production ability under visible light as well as the full solar wavelength range of light. The developed method provides a new direction towards the development of a TiO_2-based photocatalyst for visible light hydrogen production and also for other applications that can use black TiO_2.

TiO_2 has been widely studied as a semiconductor photocatalyst for hydrogen production, CO_2 reduction, and environmental pollution removal.[1–4] However, due to its large band gap (anatase, 3.2 eV and rutile, 3.0 eV), its optical absorption is confined to the ultraviolet (UV) region of the solar spectrum. Several different approaches have been carried out to enhance the light absorbance capacity and extend it towards the visible light by band gap engineering. All these efforts have enhanced the visible light absorption and the photocatalytic activity. However, the results are not up to the mark. Recently, Chen *et al.* reported black hydrogenated TiO_2 with enhanced solar light absorption.[5] Further studies on hydrogenated TiO_2 have shown significant enhancement in visible light absorption and photocatalytic activity for hydrogen production.[6–16] Different groups employed different reaction conditions and different initial TiO_2 materials to prepare hydrogenated or reduced TiO_2 with different colors like yellow, blue, gray, and black. Lu *et al.* studied the color change of commercial Degussa P25 at room temperature, employing a high pressure hydrogen (35 bar) environment.[12] Liu *et al.* reported black TiO_2 nanotube arrays converted by a high pressure H_2 treatment, with improved activity.[13] Sun *et al.* prepared black TiO_2 nanocrystals with different facets by employing high pressure.[14] Qiu *et al.* reported the rapid synthesis of blue rutile TiO_2 employing a 40 bar pressure at 450 °C.[17] Yu *et al.* prepared hydrogenated anatase TiO_2 nanosheets under a H_2 gas flow at atmospheric pressure and a temperature of 500–700 °C for various time periods to induce gradual changes in color from blue to gray.[15] Li *et al.* prepared grey mesoporous anatase TiO_2 microspheres using a hydrogen treatment process.[18] Wang *et al.* prepared temperature dependent yellowish green and black hydrogenated rutile TiO_2

Department of Energy Systems Engineering, DGIST, Daegu, 711-873, Republic of Korea. E-mail: jsyu@dgist.ac.kr

† Electronic supplementary information (ESI) available: Experimental and characterization techniques in detail, results of material characterization and photocatalysis. See DOI: 10.1039/c5ee02443a

nanowire arrays by employing ambient hydrogen pressure.[6] Naldoni *et al.* used a H_2 stream and amorphous TiO_2 to prepare black TiO_2 nanoparticles and also study the effect of the cooling process.[19] Liang *et al.* reported a hydrogenated anatase TiO_2 inverse opal structure.[20] Reduced hydrogenated TiO_2 was also prepared using ambient hydrogen–argon or nitrogen treatment at high temperature.[7,10,16,21–24] Danon *et al.* have shown the effect of reactor materials on the properties of reduced TiO_2.[23] Hoang *et al.* prepared reduced TiO_2 nanowire arrays by the co-treatment of H_2 and NH_3 and showed the synergistic effect of Ti^{3+} and N.[10] Myung *et al.* used only an argon atmosphere to prepare black TiO_2 nanoparticles using yellow TiO_2 gel at 400–600 °C.[25] To justify the enhancement of the optical properties and photocatalytic activity of black or hydrogenated TiO_2, different property factors were recognized such as surface lattice disorders, oxygen vacancies, Ti^{3+} ions, Ti–OH and Ti–H groups, and band edge shifting. However, these property factors vary, mainly depending on the synthetic methods.[11] Later on, different synthetic methods like hydrogen plasma, chemical reduction, chemical oxidation, and electrochemical reduction have been employed to obtain black TiO_2.[11,13,26–37] Other than photocatalysis, black TiO_2 also finds applications in various fields *e.g.* Li-ion batteries, Al batteries, supercapacitors, fuel cells, photoelectrochemical sensors, field emission electrodes, catalysis, and microwave absorbers.[25,29,38–44]

However, despite the dramatic enhancement of optical absorption of black TiO_2 materials, many of them do not show the expected efficiency for visible light-assisted water splitting.[8,11] This can be ascribed to the presence of several controlling factors (*vide supra*), which can also have negative effects on the photocatalytic performance. For example, surface defects and/or oxygen vacancies, considered one of the important property factors, act as electron donors to enhance donor density and improve the charge transportation in black TiO_2.[6,8] However, the high concentration of oxygen vacancies and/or surface defects can also act as charge recombination centers, which eventually decrease the photocatalytic activity.[8] Very recently, a review article on black TiO_2 materials was published by Chen *et al.*[11] describing the different synthesis methods and the improvement of different properties of black TiO_2 materials. It was suggested that "more efforts are needed from synthesis to property and application in order to finally improve the efficiency of black TiO_2 nanomaterials for practical applications in renewable energy, environment, and others". Therefore, a black TiO_2 material with optimized properties would be highly desired for visible light photocatalysis.

Herein, we report for the first time the magnesiothermic reduction of TiO_2 nanoparticles in the presence of H_2/Ar followed by acid treatment to obtain Mg-free reduced black TiO_2 nanoparticles for enhanced photocatalytic hydrogen production in the methanol–water system. Industrially, the magnesiothermic reaction has been used in the reduction chemical process, for example, reduction of silica to silicon. The reduction of titanium chloride ($TiCl_x$) in the presence of magnesium at high temperature produces metallic titanium, and the process is known as the Kroll process.[45] This is the inspiration for the present work.

We have prepared different reduced black nano TiO_2 samples by varying the molar ratio of TiO_2 and Mg, and denoted them as BT-*X* (where *X* (=0.3, 0.5, 0.6, 0.75 and 1) is the molar ratio of Mg with respect to TiO_2). Commercially available nano (10–15 nm) anatase TiO_2 (CT) was used as a precursor. For comparison, samples were also prepared in the absence of Mg (CT-H), hydrogen (BT-X-Ar), and both (CT-Ar) while keeping other parameters identical. All the prepared samples were surface-deposited with Pt nanoparticles by photoreduction and studied for photocatalytic hydrogen production in methanol–water. The experimental details and characterization techniques are provided in the ESI.†

The powder X-ray diffraction (XRD) patterns of the different samples are presented in Fig. S1 (ESI†). Mainly, the anatase phase of TiO_2 with a slight presence of the rutile phase is observed for the prepared samples. Although the XRD analysis does not indicate any major structural change during magnesium reduction except for the introduction of the rutile phase, it can be assumed that Mg changes the surface of the TiO_2 particles, which results in color changes from white to gray and black with increasing Mg (Fig. S2 for color change in the ESI†).

Raman spectroscopy was used to investigate the reduced black TiO_2 further (Fig. 1a). The Raman spectrum of CT-Ar shows 6 ($3E_g + 2B_{1g} + A_{1g}$) characteristic Raman bands of the typical anatase TiO_2 phase with the strongest Eg band around at 148 cm^{-1}. The band exhibits a blue shift accompanied by peak broadening for black TiO_2 samples compared to CT-Ar. This phenomenon was also reported earlier and attributed to non-stoichiometry over the surface of the modified TiO_2 samples and can be directly correlated to oxygen deficiency at the surface.[5–7,19,33] It could be assumed that during magnesiothermic reduction, the lattice periodicity and the octahedral symmetry of TiO_6 are destroyed on the surface. Here, it should be mentioned that the sample BT-1 shows a slight distorted spectrum, which may be due to the over-reduction and phase transition from anatase to rutile in the presence of a high amount of Mg.

The morphology of commercial nano TiO_2 (CT) and BT-0.5 was observed by high-resolution transmittance microscopy (HR-TEM) analysis. According to the images (Fig. S3, ESI†), the CT and BT-0.5 samples show a particle size around 10–20 nm. The lattice fringe pattern with a spacing of 0.35 nm confirms the (101) plane of anatase TiO_2. Here, it should be mentioned that the {101} facets of anatase TiO_2 are most active for hydrogen

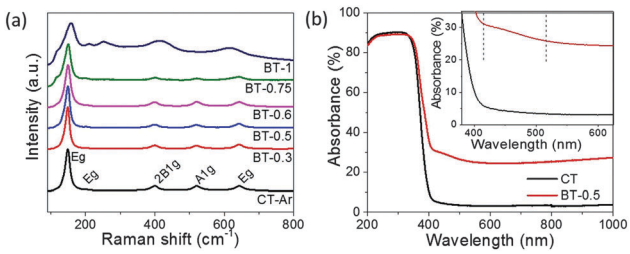

Fig. 1 Raman spectra (a) and absorption spectra (b) of the different samples. An extended absorption slope is also seen in the inset of (b).

production from water splitting in the presence of Pt as a co-catalyst.[46]

The absorption spectra (Fig. 1b) of the samples clearly depict an extended absorbance from the ultraviolet (UV) to visible (VIS) and infrared (IR) region for the Mg-treated samples (BT-0.5) compared with pristine TiO_2. The sharp absorption peak shifts to 418 nm and also displays an extended slope up to 515 nm in the visible region (see the inset of Fig. 1b). The absorption of light increases as the amount of Mg increases as observed for BT-0.75 and BT-1 in Fig. S4 (ESI†), which is also reflected in the color change trend of the samples from white to gray and black.

Therefore, magnesiothermic treatment leads to surface modification, which is reflected in enhanced light absorption as well as the color change.

The high-resolution XPS spectra of Ti 2p3/2 and Ti 2p1/2 (Fig. 2a) indicate the presence of Ti^{4+} (458.5 and 464.3 eV, respectively) for the samples CT and BT-05. The similarity of the obtained spectra indicates a similar bonding environment and the absence of any impurities like Mg or carbon after the Mg treatment of the pristine TiO_2.[5,33] There is no clear evidence of the formation of Ti^{3+} for BT-0.5. However, the Ti 2p XPS spectrum of BT-1 shows a well-formed tail towards lower binding energy due to the formation of Ti^{3+} (Fig. S5, ESI†). This result clearly indicates the formation of Ti^{3+} during the magnesiothermic treatment of TiO_2. Extrapolating this result, it can be considered that Ti^{3+} may be also formed in BT-0.5 in a lower amount. In fact, the presence of Ti^{3+} in BT-0.5 is further confirmed by the observed hysteresis in the plot of magnetic field dependence of magnetization (Fig. S6, ESI†) as the presence of Ti^{3+} introduces ferromagnetism into TiO_2.[33]

The HR-XPS spectra of O 1s (Fig. 2b) of CT and BT-05 samples show a well-developed peak at 529.8 eV, and a hump is observed at higher binding energy of ~531 eV. The peak at 529.8 eV is attributed to the lattice oxygen of TiO_2. The peak at higher binding energy indicates the presence of Ti–OH groups at the surface. The higher binding energy peak can be correlated with the oxygen vacancy or surface defects directly. It is also observed that the area of the peak at 531 eV is larger for the black TiO_2 compared with the pristine TiO_2. The peak intensity also increases with the increase of Mg amount. This can be interpreted as more oxygen vacancies created during the magnesiothermic reduction of TiO_2. Here, it should be

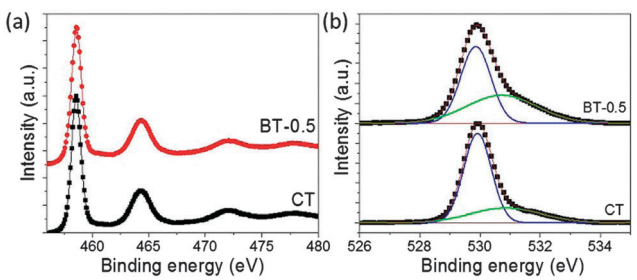

Fig. 2 High-resolution XPS for Ti 2p (a) and O 1s (b) of CT and BT-05 samples.

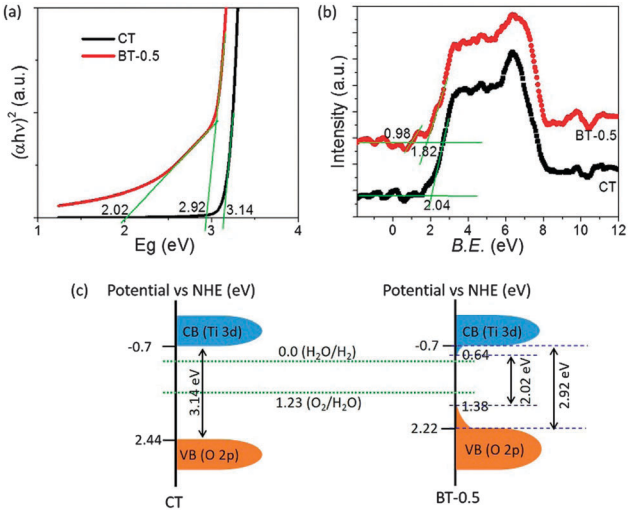

Fig. 3 (a) Tauc plot for band gap determination, (b) VB XPS of the samples, and (c) band energy diagram.

mentioned that the full XPS survey (Fig. S7a, ESI†) and Mg-scan (Fig. S7b, ESI†) of sample BT-0.5 do not show any peaks related to Mg, which further confirms that Mg is fully removed during acid treatment. However, the full XPS survey of sample BT-1 shows the presence of Mg (Fig. S8, ESI†), indicating Mg^{2+} doping of the titanium oxide framework of BT-1.

We further calculated the band gap and position of the pristine nano-TiO_2 (CT) and BT-0.5 from the Tauc plot (Fig. 3a) obtained from UV-DRS results (see the ESI†). The obtained band gap values are 3.14 and 2.92 eV for CT and BT-0.5, respectively. However, BT-0.5 shows another lower band gap value of 2.02 eV, which can be correlated to the extra slope in the absorption spectrum (inset of Fig. 1b) of BT-0.5 in the wavelength range of 418 to 515 nm. The lower band gap value of BT-0.5 suggests that a new density of states (DOS) exists as a tail of the valence band (VB) top.[19] The VB position was further analyzed through VB XPS spectra of the samples (Fig. 3b and c). The VB XPS of CT shows the position of VB top at 2.04 eV, whereas for BT-0.5 the VB top is at 1.82 eV and 0.98 eV. The VB of BT-0.5 shifts 0.22 eV and forms a tail up to 1.06 eV upward. The maximum band gap difference is 1.12 eV, which indicates another tail formation of the conduction band (CB) downward for BT-0.5. Combining the above results, a schematic illustration of the band position in the potential *vs.* NHE energy diagram for CT and BT-0.5 can be portrayed as shown in Fig. 3c. This upward shift of the VB top and the downward shift of the CB bottom are due to the presence of surface defects or oxygen vacancies and the presence of Ti^{3+}, respectively, leading to enhanced visible light absorption and expected improved photocatalytic activity.

The photocatalytic hydrogen production in methanol–water (20%) was investigated for different samples under the full solar wavelength range of light using Pt nanoparticles as co-catalysts. ~1% Pt was photo-deposited under UV light for 2 h. The deposition of Pt was confirmed by XPS (Fig. S9, ESI†) and HR-TEM (Fig. S10, ESI†) analysis of the Pt deposited BT-0.5 sample.

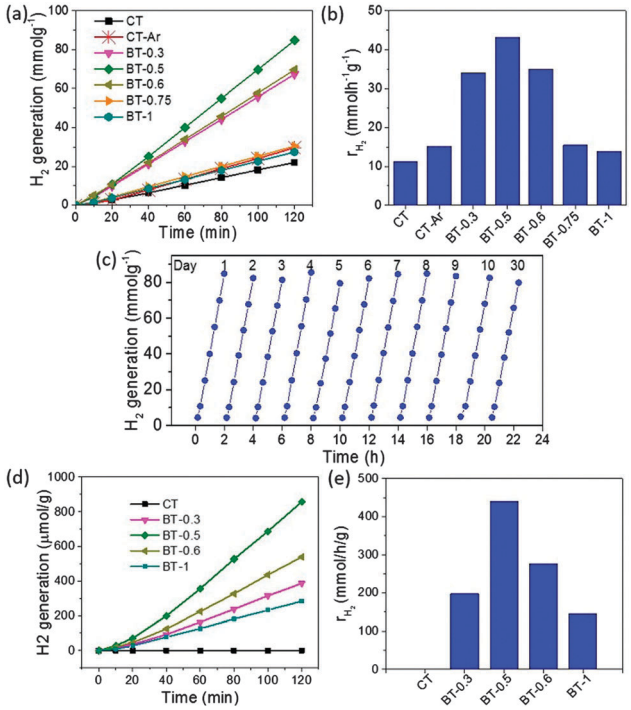

Fig. 4 H_2 generation profile (a), rate (rH_2) of hydrogen generation (b) for different samples, and the stability study of the sample BT-0.5 (c) under the full solar wavelength range of light. H_2 generation profile (d) and rate (rH_2) of hydrogen generation (e) for different samples under visible light.

The continuous hydrogen production profile and the rate of H_2 production for different samples under the full solar wavelength range of light are shown in Fig. 4a and b, respectively. The rate of hydrogen production significantly increases for the Mg-treated samples, and a maximum 43.2 mmol h^{-1} g^{-1} is observed for sample BT-0.5. This hydrogen production rate is really remarkable and is 3 to 20 times higher than the rates of similar black TiO_2 samples reported in the literature (see the ESI,† Table S1). Interestingly, the rate increases with the amount of Mg up to 0.5, and then it starts to decrease for 0.75 and 1.0 although it is observed that with the increase of the Mg amount, the sample turns more black (the absorption of light also increases) and also shows greater presence of Ti^{3+} and oxygen vacancies. One of the possible explanations for the odd results can be ascribed to the generation of new recombination sites due to over-reduction and Mg^{2+} doping in the presence of a high amount of Mg.[30,47] As a result, the hydrogen production decreases due to more hole–electron recombination although the absorption of light is high. The photoluminescence (PL) spectra (see the ESI,† Fig. S11) of the samples also indicate faster charge recombination for sample BT-1 compared with BT-0.5 and CT. Another important reason is the decrease in specific surface area with increasing Mg (see the ESI,† Fig. S12 and S13). The high surface area material can offer more active sites and improve the distribution of Pt nanoparticles to increase the overall catalytic activity. This decrease in surface area can be attributed to the increased crystallite size of the black titania with increasing Mg (see the ESI†). In addition, such a surface area decrease also results in increased Pt particle size, decreasing the efficiency of Pt.[48]

Therefore, it can be concluded that the amount of Mg plays a great role in preparing the most active photocatalyst.

Due to its outstanding photocatalytic activity, the stability of the sample BT-0.5 as a photocatalyst was further studied for hydrogen production under full solar light (Fig. 4c). It exhibits remarkable stability, as no significant decrease in the photocatalytic hydrogen production was observed in up to 10 cycles. The consistent results were collected from the same solution for 10 consecutive days. Not only this, it also shows similar photocatalytic activity even when the solution was stored and tested after 1 month. Here, it should be also mentioned that no color change was observed for all the prepared samples even after three months when stored under normal atmospheric conditions. Another interesting observation is that the developed method uses Mg and H_2 simultaneously, and both H_2 and Mg are together playing important roles to eventually generate a very active and stable reduced black titanium oxide-based photocatalyst (see the ESI,† Fig. S14).

The visible light-driven photocatalytic hydrogen production was also studied for the prepared samples (Fig. 4d and e). The activity was decreased in comparison to the full solar wavelength range of light driven activity. However, BT-05 still shows superb activity of 440 μmol h^{-1} g^{-1} compared with other Mg-treated samples and the pristine CT with no activity under visible light. Here, it should be mentioned that the poor activity of the BT-1 sample, which shows maximum absorbance in visible light (Fig. S4, ESI†) can be assigned to the low surface area and the presence of a large number of recombination centers due to Mg^{2+} doping (*vide supra*). Furthermore, the visible light activity of the magnesiothermically reduced TiO_2 sample (BT-0.5) is also superior to those of previously reported black TiO_2 samples. So far, the best rate of hydrogen production of 258 μmol h^{-1} g^{-1} was achieved by Al-reduced black S-doped rutile TiO_2 before.[34] Table S1 (see the ESI†) summarizes hydrogen generation activities under both full solar wavelength light and visible light conditions for reduced black titania samples prepared by different methods in the literature. This clearly indicates that BT-0.5 outperforms the other related samples reported earlier, demonstrating incredibly high photocatalytic hydrogen production activity under both full solar wavelength and visible light conditions.

This outstanding activity can be correlated with the extended absorption in visible light, perfect band position, the presence of an appropriate amount of Ti^{3+} and oxygen vacancies, and slower charge recombination. Here, it should be mentioned that there is a long debate on the role of Ti^{3+} in the case of reduced black TiO_2 for photocatalysis. Interestingly, there is clear evidence of the presence of Ti^{3+} in our active sample. It can be understood that the presence of Ti^{3+} in the system can reduce the recombination of the electron–hole pairs. In fact, the presence of Ti^{3+} is considered to result in the slower charge recombination in BT-0.5 as observed in the PL measurement (Fig. S11, ESI†), providing outstanding photocatalytic activity. Another important factor is the surface oxygen vacancies or disorderedness, which also seems to play a great role in increasing the absorption at higher wavelengths and eventually increasing the activity for

hydrogen production. The exposed {101} facets of BT-0.5 can also favorably influence the photocatalytic activity. On the basis of all the results, it can be claimed that the controlled magnesiothermic reduction in the presence of hydrogen is one of the best alternative ways to produce an active and stable TiO_2-based photocatalyst for hydrogen production. In the presence or absence of methanol, there is no hydrogen production without Pt as a co-catalyst. This is probably because after the generation of electrons and holes, they are prone to easily recombine with each other without Pt. However, in the case of Pt-loaded black TiO_2, in the absence of methanol, only a trace amount of hydrogen production is observed. In the absence of the sacrificial reagent, a significant amount of holes remain on the surface, which eventually recombine easily with electrons. The sacrificial reagent is used to capture the holes, which restricts the recombination of holes and electrons. More attention to optimize the system for the best photocatalytic activity and understand the origin of the improved photocatalytic activity is highly demanded. Further detailed investigation is going on in our laboratory.

In conclusion, the present work deals with the development of a novel method for the preparation of a highly active black TiO_2 photocatalyst with a low band gap, perfect band position, and slower charge recombination for visible light hydrogen production. A novel two-step process of magnesiothermic reduction in the presence of hydrogen followed by acid treatment was used for the first time to produce reduced black TiO_2. The prepared catalyst shows remarkable photocatalytic hydrogen production ability from methanol–water in the presence of $\sim$1% Pt as a co-catalyst. The maximum hydrogen production rates are 43 mmol h^{-1} g^{-1} and 440 μmol h^{-1} g^{-1} under the full solar wavelength range of light and visible light, respectively, and these values are superior to those of previously reported black TiO_2 materials. The catalyst also shows excellent stability for up to 30 days without any significant decrement in the activity. This outstanding activity and stability of our black TiO_2 suggest that a balanced combination of different factors like Ti^{3+}, surface defects, oxygen vacancies, and recombination centers is achieved along with an optimized band gap and band position during the preparation employing magnesiothermic reduction in the presence of hydrogen.

Acknowledgements

This work was supported by an NRF grant (NRF 2010-0029245) and the Global Frontier R&D Program on Centre for Multiscale Energy System (NRF-2011-0031571) funded by the Ministry of Education, Science and Technology of Korea. The authors also would like to thank KBSI at Busan for XPS measurements.

References

1 J. Schneider, M. Matsuoka, M. Takeuchi, J. Zhang, Y. Horiuchi, M. Anpo and D. W. Bahnemann, *Chem. Rev.*, 2014, **114**, 9919–9986.
2 M. Ni, M. K. H. Leung, D. Y. C. Leung and K. Sumathy, *Renewable Sustainable Energy Rev.*, 2007, **11**, 401–425.
3 Y. Qu and X. Duan, *Chem. Soc. Rev.*, 2013, **42**, 2568–2580.
4 A. Dhakshinamoorthy, S. Navalon, A. Corma and H. Garcia, *Energy Environ. Sci.*, 2012, **5**, 9217–9233.
5 X. Chen, L. Liu, P. Y. Yu and S. S. Mao, *Science*, 2011, **331**, 746–750.
6 G. Wang, H. Wang, Y. Ling, Y. Tang, X. Yang, R. C. Fitzmorris, C. Wang, J. Z. Zhang and Y. Li, *Nano Lett.*, 2011, **11**, 3026–3033.
7 Z. Zheng, B. Huang, J. Lu, Z. Wang, X. Qin, X. Zhang, Y. Dai and M.-H. Whangbo, *Chem. Commun.*, 2012, **48**, 5733–5735.
8 Y. H. Hu, *Angew. Chem., Int. Ed.*, 2012, **51**, 12410–12412.
9 W. Zhou, W. Li, J.-Q. Wang, Y. Qu, Y. Yang, Y. Xie, K. Zhang, L. Wang, H. Fu and D. Zhao, *J. Am. Chem. Soc.*, 2014, **136**, 9280–9283.
10 S. Hoang, S. P. Berglund, N. T. Hahn, A. J. Bard and C. B. Mullins, *J. Am. Chem. Soc.*, 2012, **134**, 3659–3662.
11 X. Chen, L. Liu and F. Huang, *Chem. Soc. Rev.*, 2015, **44**, 1861–1885.
12 H. Lu, B. Zhao, R. Pan, J. Yao, J. Qiu, L. Luo and Y. Liu, *RSC Adv.*, 2014, **4**, 1128–1132.
13 N. Liu, C. Schneider, D. Freitag, M. Hartmann, U. Venkatesan, J. Müller, E. Spiecker and P. Schmuki, *Nano Lett.*, 2014, **14**, 3309–3313.
14 C. Sun, Y. Jia, X.-H. Yang, H.-G. Yang, X. Yao, G. Q. Lu, A. Selloni and S. C. Smith, *J. Phys. Chem. C*, 2011, **115**, 25590–25594.
15 X. Yu, B. Kim and Y. K. Kim, *ACS Catal.*, 2013, **3**, 2479–2486.
16 Y. Zhu, D. Liu and M. Meng, *Chem. Commun.*, 2014, **50**, 6049–6051.
17 J. Qiu, S. Li, E. Gray, H. Liu, Q.-F. Gu, C. Sun, C. Lai, H. Zhao and S. Zhang, *J. Phys. Chem. C*, 2014, **118**, 8824–8830.
18 G. Li, Z. Zhang, H. Peng and K. Chen, *RSC Adv.*, 2013, **3**, 11507–11510.
19 A. Naldoni, M. Allieta, S. Santangelo, M. Marelli, F. Fabbri, S. Cappelli, C. L. Bianchi, R. Psaro and V. Dal Santo, *J. Am. Chem. Soc.*, 2012, **134**, 7600–7603.
20 Z. Liang, G. Zheng, W. Li, Z. W. Seh, H. Yao, K. Yan, D. Kong and Y. Cui, *ACS Nano*, 2014, **8**, 5249–5256.
21 Z. Wei-Dong, W. Cheng-Wei, C. Jian-Biao, L. Dong-Sheng, Z. Feng and Z. Hao-Li, *Nanotechnology*, 2012, **23**, 455204.
22 J.-Y. Shin, J. H. Joo, D. Samuelis and J. Maier, *Chem. Mater.*, 2012, **24**, 543–551.
23 A. Danon, K. Bhattacharyya, B. K. Vijayan, J. Lu, D. J. Sauter, K. A. Gray, P. C. Stair and E. Weitz, *ACS Catal.*, 2012, **2**, 45–49.
24 H. He, K. Yang, N. Wang, F. Luo and H. Chen, *J. Appl. Phys.*, 2013, **114**, 213505.
25 S.-T. Myung, M. Kikuchi, C. S. Yoon, H. Yashiro, S.-J. Kim, Y.-K. Sun and B. Scrosati, *Energy Environ. Sci.*, 2013, **6**, 2609–2614.
26 X. Chen, L. Liu, Z. Liu, M. A. Marcus, W.-C. Wang, N. A. Oyler, M. E. Grass, B. Mao, P.-A. Glans, P. Y. Yu, J. Guo and S. S. Mao, *Sci. Rep.*, 2013, **3**, 1510.
27 I. S. Cho, M. Logar, C. H. Lee, L. Cai, F. B. Prinz and X. Zheng, *Nano Lett.*, 2013, **14**, 24–31.
28 J. Dong, J. Han, Y. Liu, A. Nakajima, S. Matsushita, S. Wei and W. Gao, *ACS Appl. Mater. Interfaces*, 2014, **6**, 1385–1388.

29 Y. J. He, J. F. Peng, W. Chu, Y. Z. Li and D. G. Tong, *J. Mater. Chem. A*, 2014, **2**, 1721–1731.
30 T. Lin, C. Yang, Z. Wang, H. Yin, X. Lu, F. Huang, J. Lin, X. Xie and M. Jiang, *Energy Environ. Sci.*, 2014, **7**, 967–972.
31 T. Nakajima, T. Nakamura, K. Shinoda and T. Tsuchiya, *J. Mater. Chem. A*, 2014, **2**, 6762–6771.
32 Z. Wang, C. Yang, T. Lin, H. Yin, P. Chen, D. Wan, F. Xu, F. Huang, J. Lin, X. Xie and M. Jiang, *Adv. Funct. Mater.*, 2013, **23**, 5444–5450.
33 Z. Wang, C. Yang, T. Lin, H. Yin, P. Chen, D. Wan, F. Xu, F. Huang, J. Lin, X. Xie and M. Jiang, *Energy Environ. Sci.*, 2013, **6**, 3007–3014.
34 C. Yang, Z. Wang, T. Lin, H. Yin, X. Lü, D. Wan, T. Xu, C. Zheng, J. Lin, F. Huang, X. Xie and M. Jiang, *J. Am. Chem. Soc.*, 2013, **135**, 17831–17838.
35 G. Zhu, T. Lin, X. Lu, W. Zhao, C. Yang, Z. Wang, H. Yin, Z. Liu, F. Huang and J. Lin, *J. Mater. Chem. A*, 2013, **1**, 9650–9653.
36 H. Yin, T. Q. Lin, C. Y. Yang, Z. Wang, G. L. Zhu, T. Xu, X. M. Xie, F. Q. Huang and M. H. Jiang, *Chem. – Eur. J.*, 2013, **19**, 13313.
37 S. Tominaka, Y. Tsujimoto, Y. Matsushita and K. Yamaura, *Angew. Chem., Int. Ed.*, 2011, **50**, 7418–7421.
38 C. Barzan, E. Groppo, S. Bordiga and A. Zecchina, *ACS Catal.*, 2014, **4**, 986–989.
39 L. Zeng, W. Song, M. Li, D. Zeng and C. Xie, *Appl. Catal., B*, 2014, **147**, 490–498.
40 X. Lu, G. Wang, T. Zhai, M. Yu, J. Gan, Y. Tong and Y. Li, *Nano Lett.*, 2012, **12**, 1690–1696.
41 C. Zhang, H. Yu, Y. Li, Y. Gao, Y. Zhao, W. Song, Z. Shao and B. Yi, *ChemSusChem*, 2013, **6**, 659–666.
42 X.-Q. Zhang, J.-B. Chen, C.-W. Wang, A.-Z. Liao and X.-F. Su, *Nanotechnology*, 2015, **26**, 175705.
43 T. Xia, C. Zhang, N. A. Oyler and X. Chen, *Adv. Mater.*, 2013, **25**, 6905–6910.
44 T. Xia, Y. Cao, N. A. Oyler, J. Murowchick, L. Liu and X. Chen, *ACS Appl. Mater. Interfaces*, 2015, **7**, 10407–10413.
45 F. Habashi, *Handbook of Extractive Metallurgy*, Wiley-VCH, Weinheim, Germany, 1997.
46 T. R. Gordon, M. Cargnello, T. Paik, F. Mangolini, R. T. Weber, P. Fornasiero and C. B. Murray, *J. Am. Chem. Soc.*, 2012, **134**, 6751–6761.
47 C. Zhang, S. Chen, L. E. Mo, Y. Huang, H. Tian, L. Hu, Z. Huo, S. Dai, F. Kong and X. Pan, *J. Phys. Chem. C*, 2011, **115**, 16418–16424.
48 B. Fang, J. H. Kim, M.-S. Kim and J.-S. Yu, *Acc. Chem. Res.*, 2013, **46**, 1397–1406.

